Chemical Engineering Journal 155 (2009) 867–873

Contents lists available at ScienceDirect

Chemical Engineering Journal

journal homepage: www.elsevier.com/locate/cej

CO_2 capture from air via CaO-carbonation using a solar-driven fluidized bed reactor—Effect of temperature and water vapor concentration

V. Nikulshina[a], A. Steinfeld[a,b,*]

[a] Department of Mechanical and Process Engineering, ETH Zurich, 8092 Zurich, Switzerland
[b] Solar Technology Laboratory, Paul Scherrer Institute, CH-5232 Villigen, Switzerland

ARTICLE INFO

Article history:
Received 4 May 2009
Received in revised form
26 September 2009
Accepted 2 October 2009

Keywords:
CO_2 capture
Air
Carbonation
Kinetics
Solar energy
Radiation
Fluidized bed reactor

ABSTRACT

A two-step thermochemical cyclic process to capture CO_2 from atmospheric air via consecutive CaO-carbonation $CaCO_3$-calcination reactions is investigated using concentrated solar energy. A kinetic analysis of the carbonation of CaO with dry and moist air containing 500 ppm CO_2 is performed in a fluidized bed solar reactor with particles directly exposed to high-flux thermal irradiation. The CO_2 removal capacity was examined in the temperature range 290–390 °C and water vapor concentration range 0–17%. Complete CO_2 removal was achieved from a continuous flow of moist air at 390 °C and residence times of less than 1.5 s, while the extent of CaO-carbonation was almost doubled by the addition of water vapor. Kinetic models that account for consecutive chemically and diffusion-controlled regimes were applied to describe the carbonation rate with dry air, limited initially through interface reactions and later through reactant penetration across the layer of $CaCO_3$ until reaching the unreacted core. In contrast, a chemically-controlled rate law was applied to describe the augmented carbonation rate with moist air, which proceeded through the formation of an interface of water and/or OH ions at the solid surface not covered by $CaCO_3$. The corresponding reaction orders and Arrhenius rate constants were determined by fitting to the experimental data.

1. Introduction

In previous papers [1–3], the chemical thermodynamics, reaction kinetics, and materials recyclability were investigated for a novel thermochemical cyclic process aimed at the continuous removal of CO_2 from ambient air using concentrated solar energy as the source of high-temperature process heat. The cycle is based on consecutive CaO-carbonation and $CaCO_3$-calcination steps, through the reversible reaction:

$$CaO(s) + CO_2(g) = CaCO_3(s) \quad (1)$$

The capture of CO_2 from air – vis-à-vis its capture from a flue gas stream – is evidently a thermodynamically less favorable option. However, air remediation could become necessary for stabilizing the global CO_2 concentration in the atmosphere in view of increasing emissions derived from transportation and other distributed sources [4–7]. In this case, the CO_2 capture plant could be strategically located next to a source of renewable energy and to the final storage site, such as inhabited deserts with high solar irradiation and vast geological storage reservoirs. Calcium-based materials have been applied as CO_2 sorbents in reformers [8–10], gasifiers [11], and combustors [12–18]. Recyclability by calcination is crucial. Sorbent deactivation is mainly attributed to sintering [12–14,16–18], but reactivation is accomplished by hydration with intermediate formation of $Ca(OH)_2$ [2,3,19–21].

$$CaCO_3(s) + H_2O(g) = Ca(OH)_2(s) + CO_2(g) \quad (2)$$

The CO_2–CaO reaction proceeds through an initially rapid and chemically-controlled regime, followed by a transition to a slower diffusion-controlled regime [2,22–26]. The addition of water vapor significantly enhanced the reaction kinetics [2,27,28].

In this paper, an experimental investigation on CaO-carbonation with air is reported using a solar-driven fluidized bed reactor. Examined are the effects of the reactor temperature and water vapor concentration on the reaction kinetics and CO_2 removal capacity, with the aim of minimizing water feed and temperature level to reduce the energy penalty associated with evaporation and superheating in large-scale commercial applications. Kinetic rate laws are formulated for the reactions with dry and moist air, and their rate constants are determined by fitting to the experimental data obtained with reactants directly exposed to concentrated thermal irradiation. The results may be directly applied to guide

* Corresponding author at: Department of Mechanical and Process Engineering, ETH Zurich, Sonneggstr. 3, ML J 42.1, ETH-Zentrum, 8092 Zurich, Switzerland. Tel.: +41 44 6327929; fax: +41 44 6321065.
E-mail address: aldo.steinfeld@ethz.ch (A. Steinfeld).

1385-8947/$ – see front matter © 2009 Elsevier B.V. All rights reserved.
doi:10.1016/j.cej.2009.10.004

Nomenclature

Ar	Archimedes number
C	CO_2 concentration [ppm]
d_p	particle diameter [m]
d_p^*	dimensionless particle diameter
g	gravitational constant [N/kg]
E_a	apparent activation energy [kJ mol^{-1}]
k	kinetic rate constant [s^{-1}]
k_0	pre-exponential factor [s^{-1}]
L_0	total pore length [1/m^2]
n	number of moles
q	frequency distribution fraction [%]
$p^*_{H_2O}$	equilibrium partial pressure of water [bar]
R	ideal gas constant [J mol^{-1} K^{-1}]
R^2	coefficient of determination
Re_{mf}	Reynolds number at minimum fluidization velocity
S_0	surface area available for reaction [m^2/cm^3]
T	temperature [°C]
t	time [s]
X	reaction extent
X_u	ultimate conversion
u_{mf}	minimum fluidization velocity of binary mixture [m/s]
$u_{mf,0}$	minimum fluidization velocity of coarse particles [m/s]
u^*	dimensionless velocity
u_t	terminal fall velocity [m/s]
$u_{t,c}$	terminal fall velocity of coarse particles [m/s]
$u_{t,f}$	terminal fall velocity of fine particles [m/s]
u_t^*	dimensionless terminal velocity [m/s]
u_0	superficial gas velocity [m/s]

Greek letters

ε_0	porosity
ρ_f	density fluid [kg/m^3]
ρ_p	density particle [kg/m^3]
μ	viscosity fluid [Pa s]
Φ	sphericity

the design of solar reactors with similar heat and mass transfer characteristics.

2. Experimental set-up

The laboratory-scale solar reactor prototype is depicted in Fig. 1. The details of its design and its performance for conducting consecutive CaO-carbonation and $CaCO_3$-calcination cycles were described previously [3]. The main engineering features are summarized here. It consists of a 25 mm-o.d. 22 mm-i.d., 25 cm-height quartz tube containing a fluidized bed of CaO particles. Experimentation was carried out at the ETH's High-Flux Solar Simulator: a high-pressure Ar arc close-coupled to an elliptical reflector that delivers an external source of intense thermal radiation and simulates the heat transfer characteristics of highly concentrating solar systems [29]. With this arrangement, the fluidized bed is directly exposed to concentrated thermal radiation, providing efficient heat transfer to the reaction site. The nominal fluidized bed and off-gas temperatures were measured by thermocouples type-K. The incoming gas (synthetic air) and liquid (water) flows are controlled by electronic flow controllers (Bronkhorst HI-TEC) with the operating ranges 0–5 l/min and 0–1 l/min and an accuracy of ±2% for gas and liquid flows, respectively.

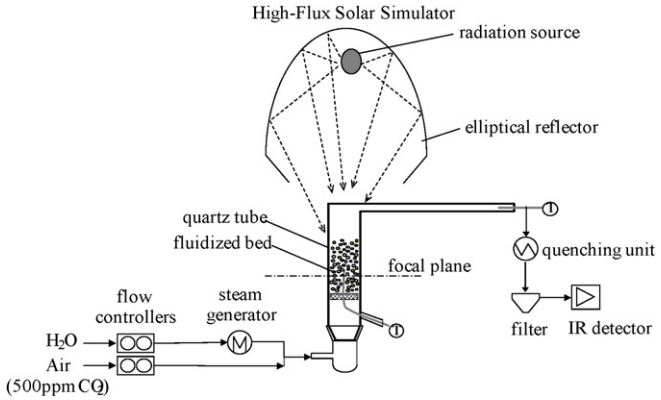

Fig. 1. Scheme of experimental set-up, featuring a fluidized bed reactor directly exposed to concentrated thermal radiation.

Synthetic air containing 500 ppm CO_2 (manufactured gas mixture of 79.5 vol% of N_2, 20.5% of O_2, 500 ppm of CO_2, <200 vpm of H_2O) was used in all experimental runs, as this concentration in the ambient air is predicted by the time the proposed technology would become indispensable. No differences in the reaction kinetics are expected if live air were used, unless contaminated with species (e.g. by-products from combustion processes) that react with $CaO/CaCO_3$. The CO_2 content of the gaseous products was analyzed by an IR system (Siemens Ultramat 23) equipped with two detectors for the ranges of 0–1000 ppm and 0–5%, at 1 Hz sampling rate and 0.2% range detection limit. Particle size distribution of solid reactants was measured by laser scattering (HORIBA LA-950 laser scattering analyzer). Specific surface area was determined by N_2 adsorption at 77K (Micromeritics TriStar 3000). Composition of solid products was determined by X-ray powder diffraction (XRD, Bruker AXS D8 Advance 40 kV, 40 mA, Å, 2θ = 10–70°, 0.05° step).

The reactor was loaded with 6.5 g of 3 wt% $CaO–SiO_2$. CaO particles were obtained by carbonation–calcination of $Ca(OH)_2$ powder (Fluka # 21181; BET specific surface = 17.4 m^2/g; average pore size 197.5 Å) using the solar-driven fluidized bed reactor, as described previously [3]. SiO_2 coarse particles (MERK #1.07711.1000; BET specific surface = 1.73 m^2/g; average pore size = 48 Å) were added to facilitate fluidization and avoid sintering. Mean particle sizes

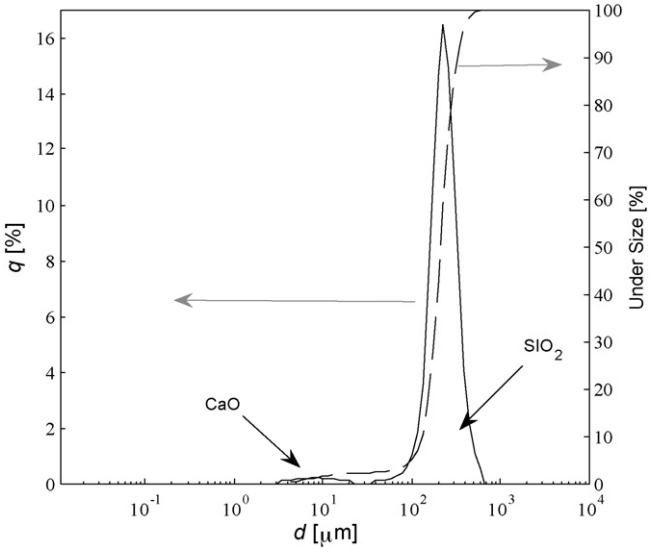

Fig. 2. Particle size distributions of binary mixture CaO/SiO_2.

Table 1
Summary of particle dynamics characterization.

	$\bar{d}_p \times 10^6$ [m]	ρ_p [kg/m^3]	Φ	$u_{mf} \times 10^2$ [m/s]	$u_t \times 10^2$ [m/s]
CaO	8	3350	0.70	–	0.634
SiO_2	200	2650	0.95	3.45	156
Mixture	–	–	–	2.76	–

of CaO and SiO_2 were 9 and 229 μm, respectively, as determined by the bimodal distribution function shown in Fig. 2. BET specific surface area of the sorbent binary mixture CaO/SiO_2 was 2.3 m^2/g with an average pore size of 94 Å. The specific surface area of CaO particles in the binary mixture, estimated from the mass fractions, was 20.7 m^2/g. The laboratory fluidized bed reactor operated reliably with the selected particle sizes. Fine powders with high specific surface area enhance the reaction kinetics, but may introduce handling complications in scaled-up reactor designs. The use of inert additives, such as SiO_2, causes an energy penalty during the calcination stage, but the binary mixture may be replaced by pelletized limestone. For a binary mixture comparable to the one used in this study, with a mass fraction of 95% of coarse particles and 5% of fines, $u_{mf}/u_{mf,0} \approx 0.8$ [30], where $u_{mf,0}$ is the minimum fluidization velocity of the coarse particles determined from [31]:

$$Ar_0 = 24.5\mathrm{Re}^2_{mf,0} + 1650\mathrm{Re}^2_{mf,0} \quad (3)$$

with

$$\mathrm{Re}^2_{mf,0} = \frac{d_{p,c} \cdot u_{mf,0} \cdot \rho_f}{\mu_f} \quad (4)$$

Hence, $u_{mf,0} = 0.0345$ m/s and $u_{mf} = 0.0276$. The terminal velocities of the single CaO and SiO_2 particles are calculated according to [32]:

$$d^* = d_p \left[\frac{\rho_f(\rho_p - \rho_f)}{\mu^2} \right]^{1/3} \quad (5)$$

$$u^* = u \left[\frac{\rho^2}{\mu(\rho_p - \rho_f)} \right]^{1/3} \quad (6)$$

$$u_t{}^* = \left[\frac{18}{(d_p^*)^2} + \frac{2.335 - 1.744\Phi}{(d_p^*)^{0.5}} \right]^{-1}, \quad 0.5 < \Phi < 1 \quad (7)$$

Assuming the SiO_2 and CaO sphericities $\Phi_{SiO_2} = 0.95$ and $\Phi_{CaO} = 0.7(32)$, the corresponding terminal velocities are $u_{t,c} = 1.56$ m/s and $u_{t,f} = 0.000634$ m/s. The results of the particle dynamics characterization are summarized in Table 1.

The fluidized bed was first heated under Ar to the desired steady-state temperature, and then exposed to the reacting gas: synthetic air ("dry air") or a mixture of synthetic air and water vapor ("moist air"). A synthetic air mass flow rate of 2 l_n/min[1] was kept constant throughout all the experiments. The temperature was varied in the range 290–390 °C. The water vapor concentration was varied in the range 0–17%. An upper limit of 17% was chosen, as this concentration was already shown in the cyclic process to result in fast CO_2 uptake [3], and lower concentrations imply a reduction in the energy penalty for water evaporation and superheating. The reaction extent of CaO-carbonation, X_{CaO}, is defined as:

$$X_{CaO} = 1 - \frac{n_{CaO}(t)}{n_{CaO,0}} \quad (8)$$

where $n_{CaO,0}$ is the initial CaO molar content and $n_{CaO(t)}$ is the CaO molar content at time t as determined from the measured CO_2 in the product gases. Equilibrium composition computations [33] indicate that the intermediate formation of $Ca(OH)_2$ is thermodynamically favorable when CaO is reacted with moist air. The partial pressure of water vapor for all performed runs, except those with the water vapor concentration of 3% and 4.9% at 390 °C, was higher than the equilibrium vapor pressure, given by $p^*_{H_2O}$ [bar] $= 8 \times 10^6 \exp(-12512/T$ [K]). Note however that the intermediate formation of $Ca(OH)_2$ by hydration of CaO is continuously consumed during carbonation [34,35], as XRD measurement confirmed that $Ca(OH)_2$ was not present in the final solid products.

3. Results and discussion

The reaction extent of CaO-carbonation with air (containing 500 ppm CO_2) at 390 °C as a function of the reaction time is shown in Fig. 3 for various water vapor concentrations in the range 0–17%. The corresponding CO_2 concentration in the outlet air flow exiting the fluidized bed is shown in Fig. 3b. For all runs at 390 °C, complete CO_2 removal is achieved from a continuous air flow at residence times of 1.1–1.3 s during a first reaction stage. This stage lasted between 1190 s at 0% H_2O–air and 1830 s at 4.9% H_2O–air. In the dry air case, the rate of CaO-carbonation varies as the reaction progresses and is initially controlled by chemical reaction and later – when a thicker product layer is formed – by diffusion [24,25]. In the moist air case, the initial linear stage corresponds to the chemically-controlled regime, while the slow-down stage corresponds to a combined chemically and diffusion-controlled regime [34,35]. Final reaction extent of CaO-carbonation with air at 390 °C as a function of water vapor concentration is shown in Fig. 3c. X_{CaO} increases from 0.35 with dry air to 0.5 with moist air containing 3% H_2O after 2500 s. At these conditions, the formation of $Ca(OH)_2$ is thermodynamically unfavorable. A further increase of the water vapor concentration to 17%, where $Ca(OH)_2$ is thermodynamically stable, has practically no influence on the final reaction extent. Thus, augmentation might not be attributed to the intermediate formation of $Ca(OH)_2$. Presumably, the catalyzing surface effect by steam is the primary driver, which is consistent with previous observations [35].

The extent of CaO-carbonation with dry air (containing 500 ppm CO_2) as a function of the reaction time is shown in Fig. 4, for isothermal runs in the range 300–390 °C. The data points are the experimentally measured values, the curves are the numerically modeled values described in the following section. The reaction is characterized by an initial rapid chemically-controlled regime followed by a transition to a diffusion-controlled regime governed by CO_2 diffusion through the solid $CaCO_3$ layer [2,24,25]. Clearly, the reaction rate in both regimes is augmented by an increase of temperature [25] leading to higher conversion and reaching $X_{CaO} = 0.35$ at 390 °C after 2500 s.

The extent of CaO-carbonation with moist air (containing 500 ppm CO_2 and 3% H_2O) as a function of the reaction time is shown in Fig. 5 for isothermal runs in the range 300–380 °C, and with moist air (containing 500 ppm CO_2 and 4.9% H_2O) as a function of the reaction time is shown in Fig. 6 for isothermal runs in the range 290–375 °C. The data points are the experimentally measured values, the curves are the numerically modeled values described in the following section. Clearly, the presence of water vapor enhances the surface kinetics by the adsorption of CO_2 on the solid surface by OH-groups [2]. As already observed in Fig. 3, an increase of the water vapor concentration from 3 to 4.9% has practically no influence on the final conversion, reaching $X_{CaO} = 0.49$–0.52 at 375–380 °C after 2500 s.

[1] l_n denotes liters at normal conditions; mass flow rates are calculated at 273 K and 1 bar.

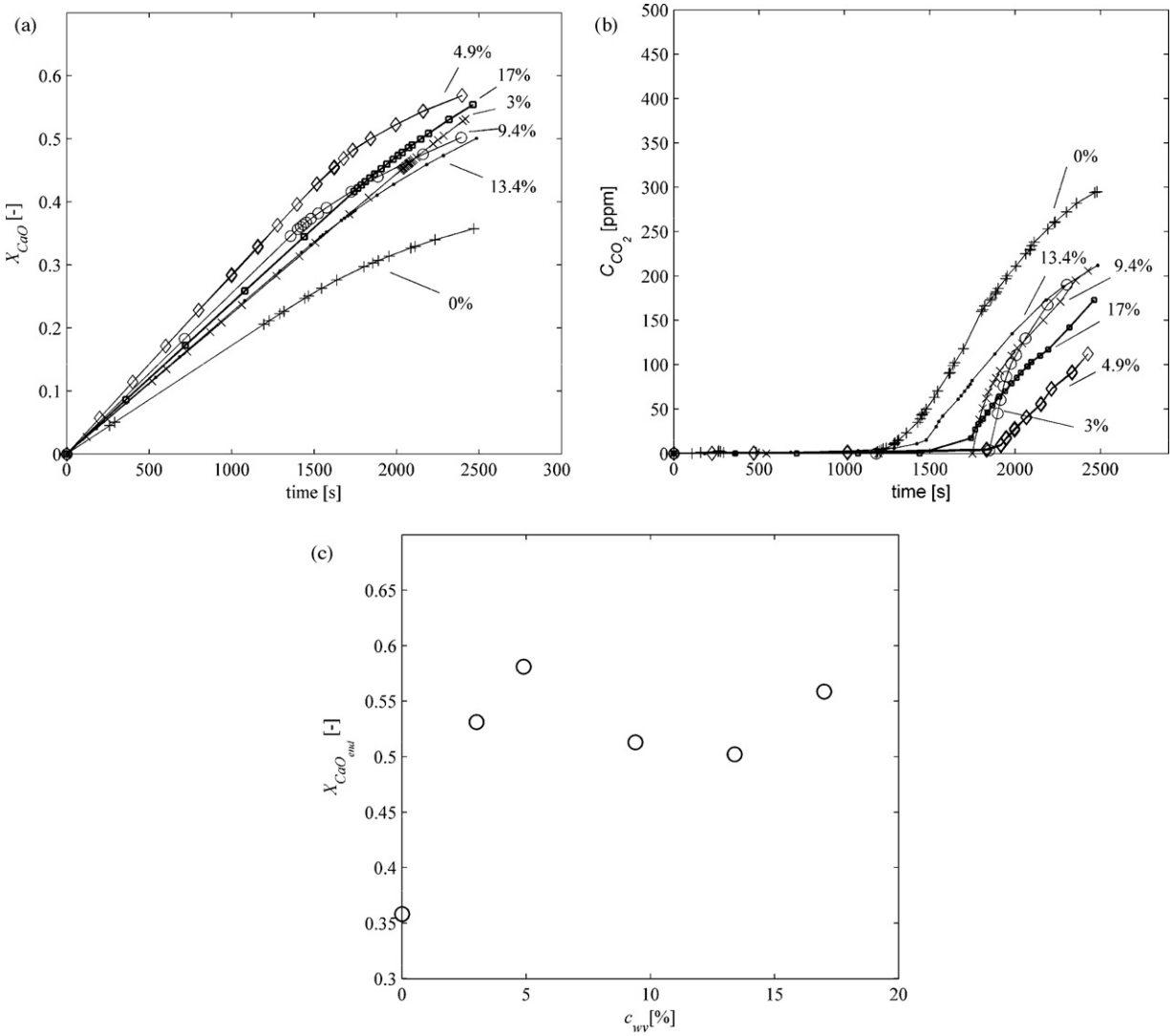

Fig. 3. (a) Extent of CaO-carbonation as a function of time at 390 °C with air containing 500 ppm CO_2; (b) corresponding CO_2 concentration in the outlet air flow exiting the fluidized bed; (c) reaction extent after 2500 s of CaO-carbonation as a function of time at 390 °C with air containing 500 ppm CO_2. The parameter is the water vapor concentration of the inlet air, in the range 0–17%.

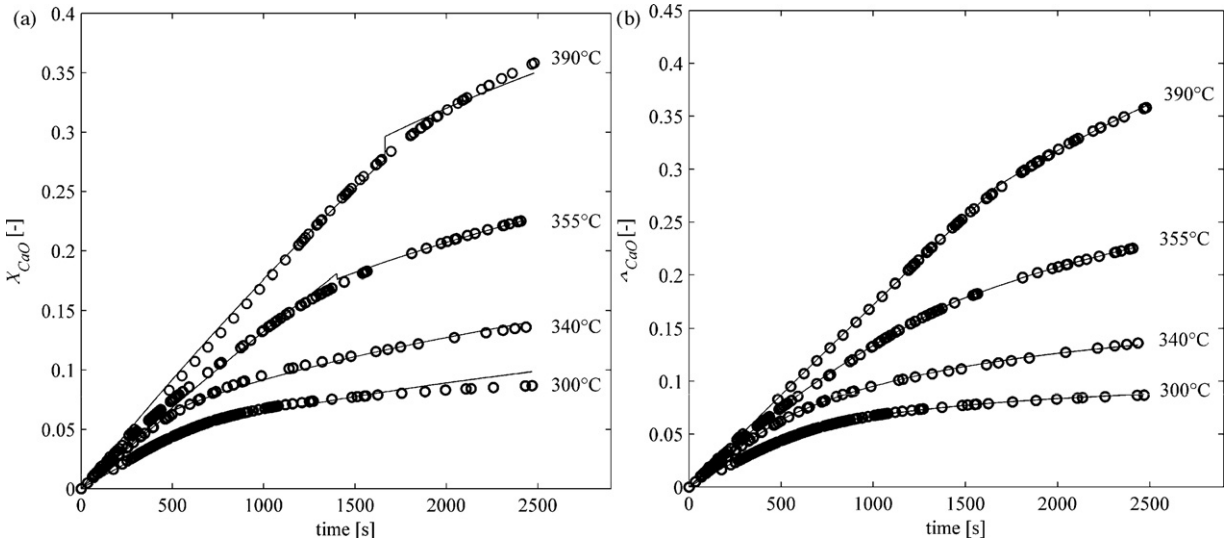

Fig. 4. Experimentally measured (data points) and numerically modeled (curves) extent of the CaO-carbonation with dry air containing 500 ppm CO_2 as a function of time for isothermal runs in the range of 300–390 °C, by applying (a) the Bhatia and Perlmutter model and (b) the Lee model.

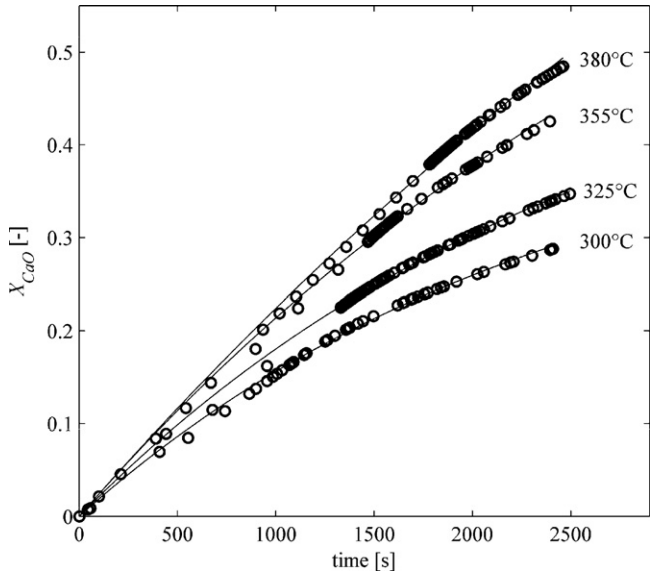

Fig. 5. Experimentally measured (data points) and numerically modeled (curves) extent of CaO-carbonation with moist air containing 500 ppm CO_2 and 3% H_2O as a function of time for the isothermal runs in the range 300°–380 °C.

4. Kinetic modeling

4.1. Dry air carbonation

Since the rate of CaO-carbonation with dry air varies with X_{CaO} (Fig. 4), the experimental data was divided into the two consecutive chemically-controlled and diffusion-controlled regimes with transition at 731, 516, 1401 and 1664 s for 300, 340, 355 and 390 °C, respectively. Firstly, Bhatia and Perlmutter's model [25], which takes into account the internal pore structure of CaO, is applied to describe the apparent kinetics of CaO-carbonation in the two regimes. It is expressed by:

for the chemically-controlled regime:

$$\frac{1}{\psi}\left[\sqrt{1-\psi\ln(1-X)}-1\right]=kt \tag{10}$$

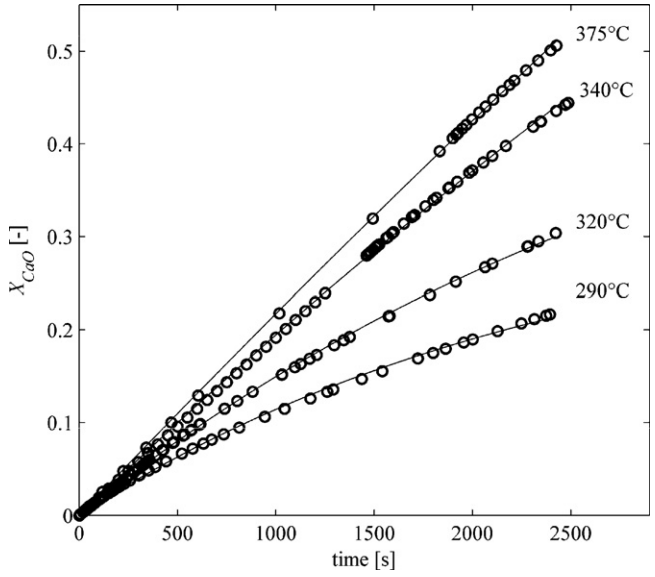

Fig. 6. Experimentally measured (data points) and numerically modeled (curves) extent of CaO-carbonation with moist air containing 500 ppm CO_2 and 4.9% H_2O as a function of time for the isothermal runs in the range 290–375 °C.

Table 2
Kinetic parameters in the consecutive chemically-controlled and diffusion-controlled regimes by applying Lee's model.

T [°C]	Chemically-controlled		Diffusion-controlled	
	k [s^{-1}]	X_u	k [s^{-1}]	X_u
300	1.06×10^{-4}	0.13	1.68×10^{-4}	0.11
340	1.48×10^{-4}	0.23	1.93×10^{-4}	0.17
355	1.69×10^{-4}	0.35	2.1×10^{-4}	0.39
390	1.7×10^{-4}	0.83	2.6×10^{-4}	0.81

for the diffusion-controlled regime:

$$\frac{1}{\psi}\left[\sqrt{1-\psi\ln(1-X)}-1\right]=k\sqrt{t} \tag{11}$$

with ψ being structural parameter defined by:

$$\psi=\frac{4\pi L_0(1-\varepsilon_0)}{S_0^2} \tag{12}$$

where L_0 is the total pore length, ε_0 is porosity, and S_0 is the surface area available for reaction. Assuming that the pore characteristics of the synthesized CaO particles are comparable to those of the initial $Ca(OH)_2$ determined by BET analysis, $L_0 = 6.65\times10^{14}$ [$1/m^2$] (assuming a cylindrical pore model), $\varepsilon_0 = 0.2$, and $S_0 = 193$ [m^2/cm^3], yielding $\psi = 0.176$. Eqs. (10) and (11) were fitted to the experimental data by varying the value of k and using an error minimization algorithm based on Nelder–Mead method [36]. The solid lines of Fig. 4a correspond to the numerically modeled X_{CaO}. The corresponding Arrhenius plots are shown in Fig. 7a. The apparent activation energies and pre-exponential factors obtained by linear fitting are: $E_{a,chem} = 8.2$ kJ mol^{-1}, $E_{a,diff} = 15.3$ kJ mol^{-1}, $k_{0,chem} = 0.0012$ s^{-1} and $k_{0,diff} = 0.43$ s^{-1} for the chemically-controlled and diffusion-controlled regimes, respectively. The coefficient of determination R^2, defined as $R^2 = \mathrm{cov}(X_{exp}, X_{model})/\mathrm{var}(X_{exp})\,\mathrm{var}(X_{model})$, is higher then 0.99 and 0.96 in the chemically and diffusion-controlled regimes accordingly for all curves considered. The divergence between the experimental and modeled data in the diffusion-controlled regime is attributed to the possible discrepancy in the morphology between the initial $Ca(OH)_2$ and the synthesized CaO.

Secondly, Lee's model [24], which was developed on Bhatia and Perlmutter's data, is also applied to describe the apparent kinetics of CaO-carbonation in the two regimes. It is expressed by:

$$\frac{dX}{dt}=k\left(1-\frac{X}{X_u}\right)^n \tag{13}$$

where n is a reaction order, and X_u is the ultimate conversion of CaO at which the rate of carbonation approaches to zero, and k is the intrinsic chemical reaction rate. Integrating Eq. (13) yields:

for the chemically-controlled regime ($n = 1$):

$$X=X_u\left(1-\exp\left(-\frac{k}{X_u}t\right)\right) \tag{14}$$

for the diffusion-controlled regime ($n = 2$):

$$X=\frac{X_u t}{(X_u/k)+t} \tag{15}$$

Eqs. (14) and (15) were fitted to the experimental data by varying the values of k and X_u using an error minimization algorithm based on Nelder–Mead method [36]. The solid lines of Fig. 4b correspond to the numerically modeled X_{CaO}. The values for k and X_u for both regimes are summarized in Table 2. The corresponding Arrhenius plots are shown in Fig. 7b. The apparent activation energies and pre-exponential factors obtained by linear fitting are: $E_{a,chem} = 4.8$ kJ mol^{-1}, $E_{a,diff} = 5.8$ kJ mol^{-1}, $k_{0,chem} = 11\times10^{-4}$ s^{-1} and $k_{0,diff} = 9.2\times10^{-4}$ s^{-1} for the chemically-controlled and diffusion-controlled regimes, respectively. In this

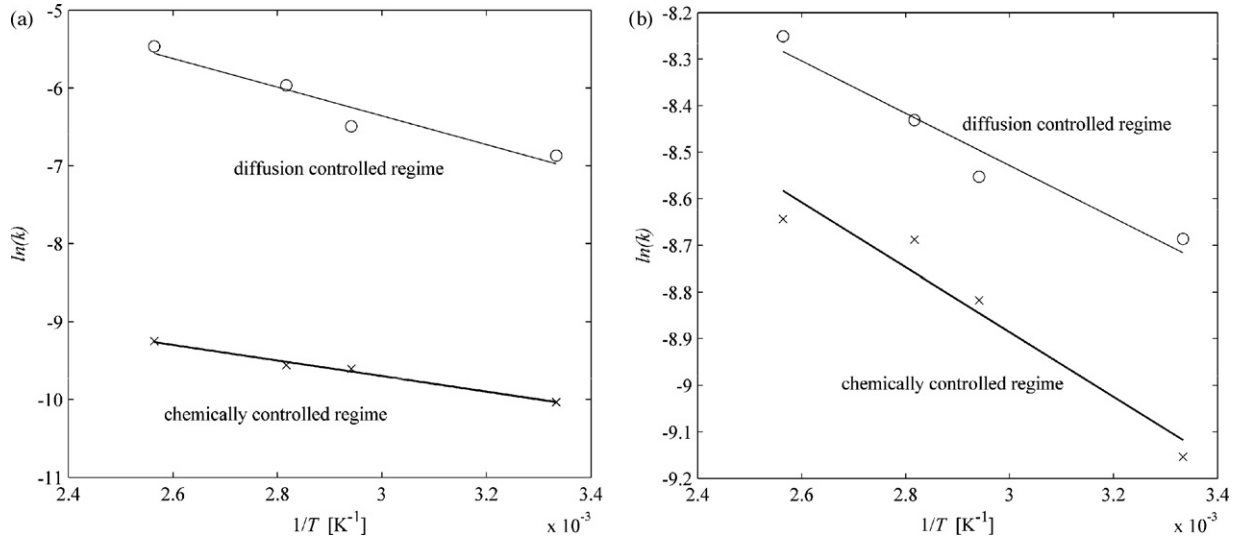

Fig. 7. Arrhenius plot for k in the chemically and diffusion-controlled regimes determined by applying (a) Bhatia and Perlmutter's model and (b) Lee's model.

case, the coefficient of determination R^2 is larger than 0.999 for all curves considered. The transition times between the regimes can be found by solving the system of Eqs. (14) and (15), yielding values comparable to those computed numerically.

The values of E_a determined by applying Bhatia and Perlmutter's model are about twice those determined by applying Lee's model. Previously reported activation energies are in the range of 39.7–89 kJ/mol for dry carbonation of lime at around 400 °C with CO_2 partial pressure in the range 10–42% and using commercially available CaO particles of average size 81 μm [24–26,37]. Since CaO particles synthesized for this study are characterized by smaller particle size and higher reacting surface area, their carbonation is less hindered by diffusion limitations and less dependent on temperature, which lead to the smaller values of the activation energy. For the chemically-controlled regime, the value of the activation energy is comparable to that for carbonation with moist air (see next section). The direct irradiation of the reactants may stimulate a photochemical enhancement of the reaction kinetics.

4.2. Moist air carbonation

Shih's model [38], appropriately applied for $Ca(OH)_2$ carbonation and for CaO-carbonation in the presence of water vapor [2], considers CO_2 adsorption by water molecules and/or OH ions at the solid surface. The reaction rate is assumed to be chemically-controlled at the $Ca(OH)_2$ surface that is not yet covered by $CaCO_3$, and is expressed by:

$$\frac{dX}{dt} = k_1 \left[[1 - (2-n)k_2 X]^{1/(2-n)} \right] \quad (16)$$

where k_1 and k_2 are proportionality constants and n is the reaction order. Eq. (16) was fitted to the experimental data for the CaO-carbonation with moist air (Figs. 5 and 6) by varying the values of k_1, k_2, and n using an error minimization algorithm based on Nelder–Mead [36]. The solid lines of Figs. 5 and 6 correspond to the numerically modeled X_{CaO}, with $R^2 > 0.99$ for both cases. The mean value for n is 1 for both experimental sets, which is consistent with an intrinsic chemical reaction rate-determining regime [38]. Eq. (16) with $n = 1$ is equivalent to Eq. (14), obtained by applying Lee's model for dry carbonation in the chemically-controlled regime [24]. The Arrhenius plots for k_1 are shown in Fig. 8. The apparent activation energies and frequency factors obtained by linear regression are $E_a = 3.02\ kJ\ mol^{-1}$, $k_0 = 0.00065\ s^{-1}$ for CaO-carbonation with moist 3% H_2O–air (Fig. 5), and $E_a = 5.15\ kJ\ mol^{-1}$, $k_0 = 0.0012\ s^{-1}$ for CaO-carbonation with moist 4.9% H_2O–air (Fig. 6). The relatively low values of E_a indicate weak dependence on temperature and are in a good agreement with previously reported data [2,38]. For example, $E_a = 17.44\ kJ\ mol^{-1}$ was obtained by thermogravimetric analysis of CaO-carbonation with CO_2 from moist (50% water vapor) ambient air [2].

4.3. Energy balance

The required thermal energy input for the complete $CaO–CaCO_3$ thermochemical cycle is $10.6\ MJ\ mol^{-1}$ of CO_2 captured, assuming 3% water feed in the air during the carbonation step and the use of heat exchangers to partially recover the sensible heat of hot air exiting during the CaO-carbonation step at 375 °C and of hot CO_2 exiting during $CaCO_3$-calcination step at 875 °C [1,3]. For both steps of the cycle, high-temperature process heat is supplied by concentrated solar radiation. Reported energy requirements for wet scrubbing using alkali metal hydroxides solutions ranged from 30 to $390\ kJ\ mol^{-1}$ of CO_2 captured [39]. Since a significant

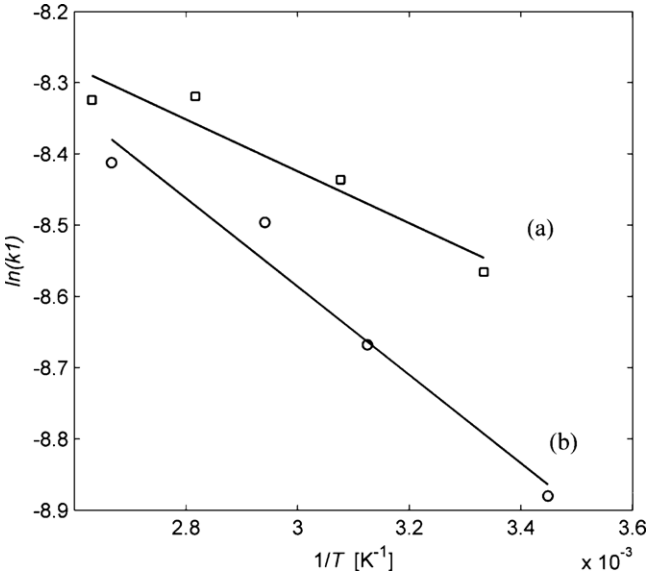

Fig. 8. (a) CaO-carbonation with moist 3% H_2O–air (Fig. 5); (b) CaO-carbonation with moist 4.9% H_2O–air (Fig. 6).

input of thermal energy is required to heat (to 375 °C) 57.9 kg of ambient air per mole CO_2, the total energy requirement for the CaO–$CaCO_3$ thermochemical cycle is estimated to be an order of magnitude higher. For a 55 MW_{th} solar power plant based on central-receiver tower technology, similar to the existing commercial plant in Seville, Spain [40], the captured rate would be 6.6 tons of CO_2 per day. Captured CO_2 could be either stored or recycled. Thermal splitting of CO_2 into separate streams of CO and O_2 has been demonstrated using metal oxide redox reactions [41,42].

5. Conclusions

We have performed a kinetic analysis on the CO_2 capture from air using a solar-driven fluidized bed reactor, in which directly irradiated CaO particles were fluidized with dry and moist air. The presence of steam significantly enhanced the surface kinetics by the adsorption of CO_2 on the solid surface by OH-groups, but a variation of the H_2O-concentration in the range 3–17% had only a weak influence on the CO_2 uptake. In contrast, CaO-carbonation with dry air was hindered by product layer diffusion. The CaO-carbonation extent reached 0.58 and 0.35 at 390 °C after 2500 s for moist and dry air, respectively. Kinetic models that account for successive chemically and diffusion-controlled regimes were applied, and reaction orders, activation energies, and pre-exponential factors were determined by fitting to the experimental data with good accuracy. The required solar thermal energy input for the complete CaO–$CaCO_3$ thermochemical cycle was calculated to be 10.6 MJ mol^{-1} of CO_2 captured, assuming 3% H_2O–air during the carbonation step and the use of heat exchangers to partially recover the sensible heat of hot air exiting during the CaO-carbonation step at 375 °C and of hot CO_2 exiting during $CaCO_3$-calcination step at 875 °C.

References

[1] V. Nikulshina, D. Hirsch, M. Mazzotti, A. Steinfeld, CO_2 capture from air and co-production of H2 via the $Ca(OH)_2$–$CaCO_3$ cycle using concentrated solar power—thermodynamic analysis, Energy 31 (2006) 1715–1725.
[2] V. Nikulshina, E. Gálvez, A. Steinfeld, Kinetic analysis of the carbonation reactions for the capture of CO_2 from air via the $Ca(OH)_2$–$CaCO_3$–CaO solar thermochemical cycle, Chem. Eng. J. 129 (2007) 75–83.
[3] V. Nikulshina, C. Gebald, A. Steinfeld, CO_2 capture from atmospheric air via consecutive CaO-carbonation and $CaCO_3$-calcination cycles in a fluidized-bed solar reactor, Chem. Eng. J. 146 (2009) 244–248.
[4] Intergovernmental Panel on Climate Change, IPCC Emissions Scenarios, Special Report, 2006.
[5] F. Zeman, Energy and material balance of CO_2 capture from ambient air, Environ. Sci. Technol. 41 (2007) 7558–7563.
[6] S. Lackner, A guide to CO_2 sequestration, Science 300 (2003) 1677–1678.
[7] D. Keith, M. Ha-Duong, J.K. Stolaroff, Climate strategy with CO_2 capture from the air, Clim. Change 74 (2006) 17–45.
[8] C. Han, D.P. Harrison, Simultaneous shift reaction and carbon dioxide separation for the direct production of hydrogen, Chem. Eng. Sci. 49 (1994) 5875–5883.
[9] B. Balasubramanian, A.L. Ortiz, S. Kaytakoglu, D.P. Harrison, Hydrogen from methane in a single-step process, Chem. Eng. Sci. 54 (1999) 3543–3552.
[10] A.L. Ortiz, D.P. Harrison, Hydrogen production using sorption-enhanced reaction, Ind. Eng. Chem. Res. 40 (2001) 5102–5109.
[11] S. Lin, M. Harada, Y. Suzuki, H. Hatano, Hydrogen production from coal by separating carbon dioxide during gasification, Fuel 81 (16) (2002) 2079–2085.
[12] C. Salvador, D. Lu, E.J. Anthony, J.C. Abanades, Enhancement of CaO for CO_2 capture in an FBC environment, Chem. Eng. J. 96 (2003) 187–195.
[13] T. Shimizu, T. Hirama, H. Hosoda, K. Kitano, M. Inagaki, K. Tejima, A twin fluid-bed reactor for removal of CO_2 from combustion processes, Trans IChemE 442 77A (1999) 62–68.
[14] J.C. Abanades, D. Alvarez, Conversion limits in the reaction of CO_2 with lime, Energy Fuel 17 (2003) 308–315.
[15] J.C. Abanades, E.J. Anthony, D.Y. Lu, C. Salvador, D. Alvarez, Capture of CO_2 from combustion gases in a fluidized bed of CaO, AIChE J. 50 (2004) 1614–1622.
[16] J.C. Abanades, The maximum capture efficiency of CO_2 using a calcination/carbonation cycle of CaO/$CaCO_3$, Chem. Eng. J. 90 (2002) 303–306.
[17] P.S. Fennell, R. Pacciani, J.S. Dennis, J.F. Davidson, A.N. Hayhurst, The effects of repeated cycles of calcination and carbonation on a variety of different limestones, as measured in a hot fluidized bed of sand, Energy Fuel 21 (2007) 2072–2081.
[18] P. Sun, J.R. Grace, C.J. Lim, E.J. Anthony, The effect of CaO sintering on cyclic CO capture in energy systems, AIChE J. 53 (2007) 2432–2442.
[19] V. Manovic, E.J. Anthony, Sequential SO_2/CO_2 capture enhanced by steam reactivation of a CaO-based sorbent, Fuel 87 (2008) 1564–1573.
[20] V. Manovic, E.J. Anthony, Steam reactivation of spent CaO-based sorbent for multiple CO_2 capture cycles, Environ. Sci. Technol. 41 (2007) 1420–1425.
[21] P.S. Fennell, J.F. Davidson, J.S. Dennis, A.N. Hayhurst, Regeneration of sintered limestone sorbents for the sequestration of CO_2 from combustion and other systems, J. Energy Inst. 80 (2007) 116–119.
[22] J.S. Dennis, A.N. Hayhurst, The effect of CO_2 on the kinetics and extent of calcination of limestone and dolomite particles in fluidised beds, Chem. Eng. Sci. 42 (1987) 2361–2372.
[23] D. Cazorla-Amoros, J.P. Joly, A. Linares-Solano, A. Marcilla-Gomis, C. Salinas-Martinez de Lecea, CO_2–CaO surface and bulk reactions: thermodynamic and kinetic approach, J. Phys. Chem. 95 (1991) 6611–6617.
[24] D. Lee, An apparent kinetic model for the carbonation of calcium oxide by carbon dioxide, Chem. Eng. J. 100 (2004) 71–77.
[25] S.K. Bhatia, D.D. Perlmutter, Effect of the product layer on the kinetics of the CO_2–lime reaction, AIChE J. 29 (1983) 79–86.
[26] H. Gupta, L.S. Fan, Carbonation–calcination cycle using high reactivity calcium oxide for carbon dioxide separation from flue gas, Ind. Eng. Chem. Res. 41 (2002) 4035–4042.
[27] K. Kuramoto, S. Fujimoto, A. Morita, S. Shibano, Y. Suzuki, H. Hatano, S.Y. Lin, M. Harada, T. Takarada, Repetitive carbonation–calcination reactions of Ca-based sorbents for efficient CO_2 sorption at elevated temperatures and pressures, Ind. Eng. Chem. Res. 42 (2003) 975–981.
[28] S. Dobner, L. Sterns, R. Graff, A. Squires, Cyclic calcination and recarbonation of calcined dolomite, Ind. Eng. Chem. Proc. Des. Dev. 16 (1977) 479–483.
[29] D. Hirsch, P.V. Zedtwitz, T. Osinga, J. Kinamore, A. Steinfeld, A new 75 kW High-Flux Solar Simulator for high-temperature thermal and thermochemical research, ASME J. Solar Energy Eng. 125 (2003) 117–120.
[30] N. Nakagawa, Minimum fluidization velocity of binary particle mixtures with adhesive fine powder, J. Chem. Eng. Jpn. 35 (2002) 595–603.
[31] C.Y. Wen, Y.H. Yu, Mechanics of fluidization, Chem. Eng. Prog. Syrup. 62 (1966) 100.
[32] A. Haider, O. Levenspiel, Drag coefficient and terminal velocity of spherical and non-spherical particles, Powder Technol. 58 (1989) 63–70.
[33] A. Roine, Outokumpu HSC Chemistry for Windows Pori, Outokumpu Research, Finland, 1997.
[34] H.S. Song, C.H. Kim, The effect of surface carbonation on the hydration of CaO, Cement Concrete Res. 20 (1990) 815–823.
[35] S. Yang, Y. Xiao, Steam catalysis in CaO carbonation under low steam partial pressure, Ind. Eng. Chem. Res. 47 (2008) 4043–4048.
[36] Matlab R2007b, The MathWorks Inc., Boston, MA, 2007.
[37] A. Dedman, A. Owen, Calcium cyanamide synthesis. Part4. The reaction $CaO + CO_2 = CaCO_3$, Trans. Faraday Soc. 58 (1962) 2027–2035.
[38] S.M. Shih, C.S. Ho, Y.S. Song, J.P. Lin, Kinetics of the reaction of $Ca(OH)_2$ with CO_2 at low temperature, Ind. Eng. Chem. Res. 38 (1999) 1316–1322.
[39] J. Stolaroff, D. Keith, G. Lowry, Carbon dioxide capture from atmospheric air using sodium hydroxide spray, Environ. Sci. Technol. 42 (2008) 2728–2735.
[40] R. Osuna, V. Fernández-Quero, M. Sánchez, Plataforma solar sanlúcar la mayor: The largest European solar power Site 14th Biennial Solar PACES Symposium, Las Vegas, March 4–7, 2008.
[41] M.E. Gálvez, P. Loutzenhiser, I. Hischier, A. Steinfeld, CO_2 splitting via 2-step solar thermochemical cycles with Zn/ZnO and FeO/Fe_3O_4 redox reactions, Thermodynam. Anal. Energy Fuels 22 (2008) 3544–3550.
[42] P. Loutzenhiser, M.E. Galvez, I. Hischier, A. Stamatiou, A. Frei, A. Steinfeld, CO_2 splitting via two-step solar thermochemical cycles with Zn/ZnO and FeO/Fe_3O_4 redox reactions II, Kinetic Anal Energy Fuels 23 (2009) 2832–2839.